Ga droplet morphology on GaAs(001) studied by Lloyd's mirror photoemission electron microscopy

2009 J. Phys.: Condens. Matter 21 314022

(http://iopscience.iop.org/0953-8984/21/31/314022)

J. Phys.: Condens. Matter **21** (2009) 314022 (5pp) doi:10.1088/0953-8984/21/31/314022

Ga droplet morphology on GaAs(001) studied by Lloyd's mirror photoemission electron microscopy

W X Tang[1], D E Jesson[1], K M Pavlov[1,2], M J Morgan[1] and B F Usher[3]

[1] School of Physics, Monash University, Victoria 3800, Australia
[2] Physics and Electronics, School of Science and Technology, University of New England, NSW 2351, Australia
[3] Department of Electronic Engineering, La Trobe University, Victoria 3086, Australia

Received 10 October 2008, in final form 25 November 2008
Published 7 July 2009
Online at stacks.iop.org/JPhysCM/21/314022

Abstract

We apply Lloyd's mirror photoemission electron microscopy (PEEM) to study the surface shape of Ga droplets on GaAs(001). An unusual rectangular-based droplet shape is identified and the contact angle is determined *in situ*. It is shown that quenching does not appreciably affect droplet shape and *ex situ* measurements of the contact angle by atomic force microscopy are in good agreement with Lloyd's mirror PEEM. Extension of Lloyd's mirror technique to reconstruct general three-dimensional (3D) surface shapes and the potential use of synchrotron radiation to improve vertical resolution is discussed.

(Some figures in this article are in colour only in the electronic version)

1. Introduction

Ga droplets on GaAs(001) have received considerable attention over the years. Langmuir decomposition of GaAs(001), in which the surface freely evaporates into a vacuum, is a prototypical example of a surface phase separation process [1–3]. For a substantial temperature range, the evaporation is congruent such that compound stoichiometry is preserved. However, above the so-called congruent evaporation temperature the rate of As evaporation from the surface exceeds that of Ga leaving behind Ga-rich liquid droplets [4, 5]. Ga droplet formation has important practical implications for homoepitaxial growth conditions [3] and understanding aspects of GaAs surface thermodynamics [6]. The evolution of droplet size distributions in the coalescence regime has also provided a model experimental system to test theoretical predictions of self-similar cluster size distributions [4]. Interestingly, size distributions appear to agree well with Monte Carlo simulations despite obvious departures from the assumptions underlying the theoretical models [7].

More recently, there has been renewed interest in the area of Ga droplets in the context of droplet epitaxy [8–14] which has been proposed as an alternative to strain-driven quantum dot (QD) formation based on the Stranski–Krastanow (SK) growth mode [15]. This method of epitaxy consists of two main stages. First, liquid Ga or In droplets are deposited on the GaAs surface. This is followed by crystallization and subsequent transformation into QDs under As pressure. Droplet epitaxy is more flexible than strain-driven SK QD formation with regard to the choice of material. For example, unstrained GaAs QDs [8, 9], InGaAs QDs with controlled In content [10] and InAs QDs [11] have all been successfully fabricated using the technique. In addition, droplet epitaxial formation of novel quantum-like structures including QD molecules [9], rings [12] and double-rings [8, 13] has recently been demonstrated. This control over shape offers exciting prospects for creating new structures with atom-like properties for novel applications in quantum computing and quantum cryptography.

Given the current interest in Ga droplets, in this paper we study the 3D morphology of droplets on GaAs(001) using Lloyd's mirror photoemission electron microscopy (PEEM). These results are compared with *ex situ* atomic force microscopy (AFM) of quenched samples. The potential of Lloyd's mirror PEEM to study dynamic events such as droplet coalescence and the advantages of using synchrotron radiation to improve resolution are discussed.

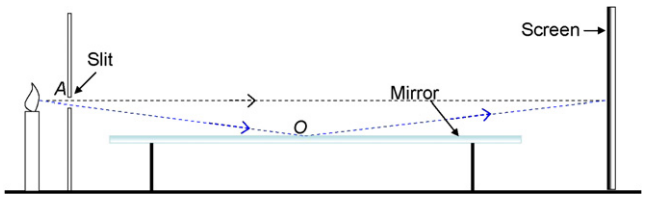

Figure 1. Schematic diagram of Lloyd's mirror. An interference pattern is formed on a screen from a superposition of light from a source at A and its reflection in a plane mirror at O.

2. Experimental details

Our ability to understand surfaces as dynamic systems has been greatly enhanced by surface electron microscopy utilizing low energy electrons [16, 17]. Important imaging modes include diffraction and phase contrast low energy electron microscopy (LEEM) [16, 18], PEEM [19, 20] and mirror electron microscopy (MEM) [21, 22]. These highly complementary techniques allow the study of surfaces *in situ* during growth and annealing. However, a major challenge common to all of these methods is the ability to extract 3D topographical data. Indeed, it is well appreciated that the cathode immersion lens, where the sample surface forms an integral part of the electron-optics [23–25], can significantly distort 3D objects. Recently, Lloyd's mirror PEEM technique [26] has been proposed to overcome some of these limitations and since it conforms to the standard geometry for threshold emission PEEM it is highly complementary to LEEM, MEM and conventional PEEM.

2.1. Lloyd's mirror PEEM

The basic principle of the classic 19th century optics experiment known as 'Lloyd's mirror' is outlined in figure 1. An interference pattern on a screen is formed from the superposition of light from a point source at A with its reflection in a plane mirror at O [27]. This simple diffraction geometry has found important practical significance across a diversity of areas ranging from astronomical interferometry [28] and high resolution lithography [29] to understanding collisions between ships and marine mammals [30]. Lloyd's mirror geometry can be easily applied to surface electron microscopy by replacing the light source with a mercury lamp source, the mirror with a planar substrate and the screen with a 3D surface object. Lloyd's fringes projected onto the object will therefore modulate electron photoemission and can be imaged in a surface electron microscope [26].

Let us first consider the geometry of the interference pattern on a 3D surface object formed by interference between the incident photon beam with its reflection from the substrate. In the case of threshold photoemission, the electron excitation is dominated by a single broadened emission line of mean wavelength $\bar{\lambda}$. Provided the illumination aperture diameter is appreciably smaller than the aperture–object distance, then the fringe intensity at a position on the 3D object surface depends only on the z-coordinate (height) of that position. In particular, the height difference Δz between fringe intensity maxima is, to a good approximation, given by [26]

$$\Delta z = \frac{\bar{\lambda}}{2\sin\alpha}, \tag{1}$$

where α is the angle of incidence of the radiation on the surface. Lloyd's fringes can therefore be used to determine the shape of a surface object.

It is important to relate the incident radiation interference pattern at the object surface, for which equation (1) is directly applicable, to the observed Lloyd's fringe pattern in PEEM. Since Lloyd's fringe spacing is significantly greater than the mean free-path $\bar{\ell}$ of electrons in the solid, we may therefore assume that all of the emitted electron flux from a position on the surface occurs locally and is proportional to the incident radiation. It is well appreciated, however, that PEEM images from 3D surface objects can be significantly distorted [23–25]. This is because non-uniform surface topography deforms the uniform electric field which influences the photo-emitted electron trajectories. We must therefore take these fringe shifts into account when reconstructing surface shape via equation (1).

The fringe shifts on the PEEM screen have been evaluated by Nepijko *et al* [23, 25] to be

$$S_x(x, y) = \frac{1}{E_o}\int_0^\infty \frac{\partial\Phi(x, y, z)}{\partial x}\,\mathrm{d}z, \tag{2}$$

where $\Phi(x, y, z)$ is the potential distribution above the object surface and E_o is the uniform electric field that accelerates the electrons across the specimen–anode aperture gap. Here we take x, y to be Cartesian coordinates within the surface plane and z is perpendicular to the surface. A surface height function $h(x, y)$ is known to produce an electric field perturbation in its vicinity, which is equivalent to the field from a planar potential distribution $\Phi(x, y, z = 0) = E_o h(x, y)$. The potential is determined from the solution to Laplace's equation with this boundary condition (i.e. the corresponding Dirichlet problem for a half-space). Substituting this solution into equation (2) and integrating over the variable z one obtains

$$S_x(x, y) = \frac{1}{2\pi}\int_{-\infty}^{+\infty}\int_{-\infty}^{+\infty} \frac{\xi h(x-\xi, y-\eta)}{(\xi^2+\eta^2)^{3/2}}\,\mathrm{d}\xi\,\mathrm{d}\eta, \tag{3}$$

where the integration variables ξ and η correspond to the x and y coordinates, respectively. If the surface potential depends only on the x coordinate then the electron shift reduces to the Hilbert transform of the object function [25]:

$$S_x(x) = -\frac{1}{\pi}\int_{-\infty}^{+\infty} \frac{h(\xi)}{x-\xi}\,\mathrm{d}\xi. \tag{4}$$

For the general and 1D cases respectively, equations (3) and (4) provide a prescription for correcting for the fringe shifts and therefore a means to reconstruct the surface shape via equation (1).

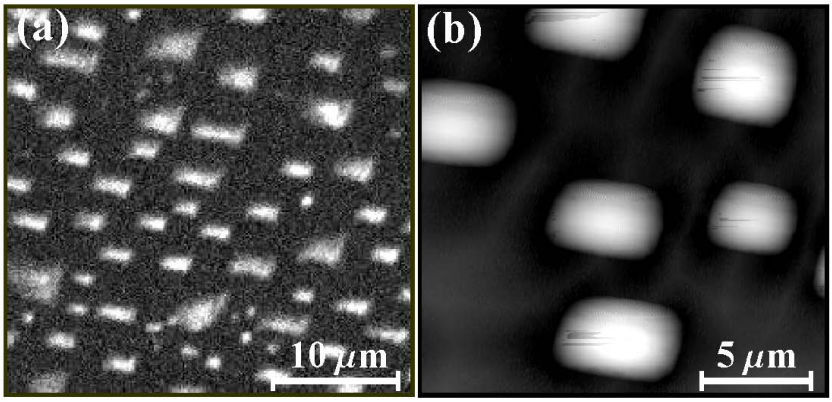

Figure 2. (a) PEEM image of Ga droplets on GaAs(001) at 660 °C. (b) *Ex situ* AFM image of the same sample following quenching to 27 °C.

2.2. Surface preparation

Two types of GaAs(001) samples were studied. One set was prepared by standard degreasing and chemical etching of 1 cm^2 portions of a GaAs(001) epi-ready wafer. Samples were introduced into a molecular beam epitaxy (MBE) system growth chamber, with a residual background pressure of less that 10^{-10} Torr. This was followed by thermal deoxidation at an As_4 pressure of 10^{-6} Torr to avoid gallium droplet formation and the growth of a 150 nm thick GaAs epilayer at 530 °C. The sample was then cooled to room temperature and capped with an amorphous arsenic layer to protect it from oxidation upon removal from the MBE chamber. Samples were transferred to the ultra-high vacuum microscope chamber and the As cap was desorbed *in situ* at 250 °C.

The second set involved annealing an epi-ready sample *in situ*. An undoped GaAs(001) epi-ready wafer of miscut less than 0.1° was degassed at 300 °C in ultra-high vacuum for 24 h combined with high temperature flashing up to 600 °C. The sample was then annealed at 580 °C for 2 h to remove the oxide layer on the surface. Ga droplets were produced by high temperature annealing above the congruent temperature [3–6].

Experiments were performed in an Elmitec LEEM III system using a 100 W UV Hg arc-discharge lamp. The electric field used for accelerating the electrons is 20 kV across a 2 mm specimen–anode gap. The base pressure of the system is below 2×10^{-10} Torr and typical pressures observed during imaging at annealing temperatures of 620 °C are in the range 7×10^{-9} Torr. The angle of the incident photons is $\alpha = 16°$, with an upper cut-off energy of the Hg arc-discharge lamp approaching 5.0 eV. As the photoemission threshold for liquid Ga is 4.33 eV [31], the emission is dominated by a single broadened emission line at $\bar{\lambda} = 253.65$ nm with $\Delta\lambda = 20$ nm.

3. Results and discussion

Upon annealing the GaAs(001) surfaces to 650 °C, which is above the congruent evaporation temperature ($T_c \sim 625$ °C [3]), a rectangular-based droplet morphology was observed *in situ* by PEEM (figure 2(a)) and *ex situ* by AFM following quenching (figure 2(b)). The rectangular-base geometry appeared to be more prevalent in the temperature range of 650–680 °C. There is a clear tendency for the solid–liquid interface to form contact lines along ⟨110⟩ crystallographic directions. A transition between ⟨110⟩ and curved segments of the contact-line occurs as droplets spread and it is therefore of interest to determine the instantaneous contact angle θ_t with a view to understanding the local energetics of metastable configurations. Lloyd's mirror PEEM offers a direct means of reconstructing the geometry of the contact-line dynamics. Figure 3(a) contains a PEEM image of part of a rectangular droplet showing Lloyd's fringes. To a good approximation, the surface profile along the white line in the figure can be regarded as 1D and so we can use the inverse Hilbert transform (equation (4)) to reconstruct the surface shape along the line from the fringe positions. This is achieved

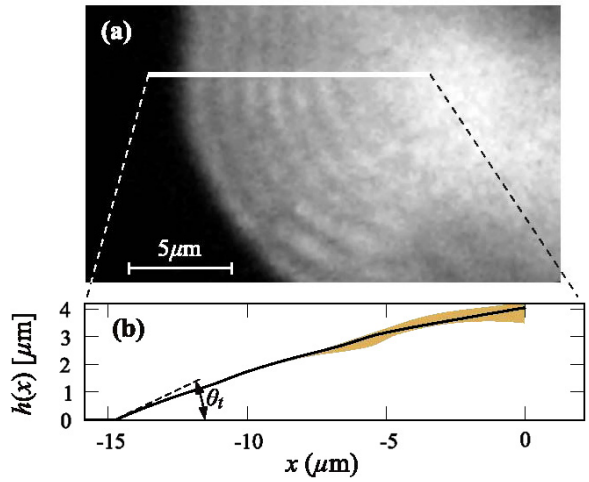

Figure 3. (a) PEEM image of part of a rectangular droplet showing bright Lloyd's fringes. (b) Reconstructed shape function obtained by an iterative method based on the inverse Hilbert transform of equation (4), from which the contact angle for the Ga droplets is $\theta_t = 22°$. Eight fringes are included in the iteration. The shaded portion of the reconstructed profile shows the range of profile variation when the two bright fringes closest to the top of the droplet are successively removed from the data. This reduction in fringe number does not significantly influence the reconstructed contact-line region.

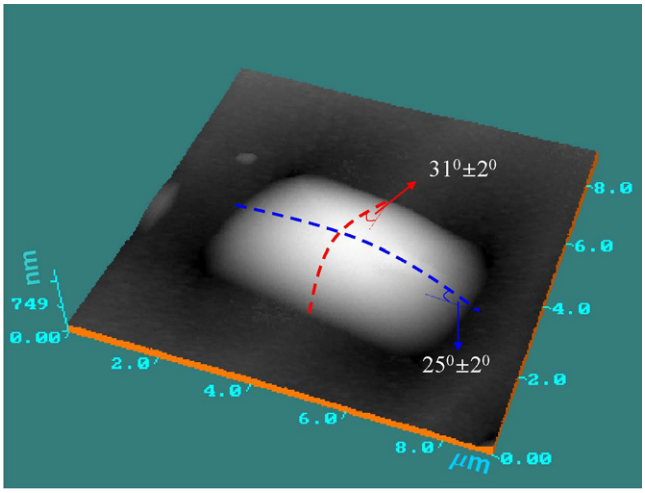

Figure 4. AFM image of a Ga droplet following quenching from 620 to 27 °C. Height profiles of the droplet along shorter ([110]) and longer ([1$\bar{1}$0]) sides of the base are shown as dashed-lines and are associated with contact angles of 31° ± 2° and 25° ± 2°, respectively.

via an iterative procedure, giving the interpolated height for the droplet shape function as shown in figure 3(b) [26]. From this we are able to deduce the contact angle for the Ga droplet as $\theta_t = 22°$, which has important implications for the physical processes governing the local stability of the contact-line [26].

We now compare droplet shape determined by Lloyd's mirror PEEM and AFM. An AFM image of a droplet captured by non-contact mode is shown in figure 4. The height profile indicates that the contact angle along the shorter side of the droplet is 25° ± 2°, while, the angle along the longer side of the droplet is 31° ± 2°. This result is in excellent agreement with Lloyd's mirror PEEM results in which the shorter side contact angle was determined to be 22° ± 2° at 620 °C (see figure 3) [26]. This agreement is perhaps surprising given the quenching and solidification of the droplet as well as surface oxidation following removal of the sample from the UHV LEEM chamber.

3.1. Towards a full reconstruction of surface topography

The viability and potential of Lloyd's mirror PEEM has been demonstrated by reconstructing a pseudo-1D droplet shape function (see figure 3(b)). We now discuss the potential to extend the technique to a full reconstruction of surface topography. This would allow us to obtain real-time movies of 3D shape evolution during dynamic events such as droplet coalescence. PEEM images taken from a movie of droplet coalescence are contained in figure 5. Initially, in figure 5(a), the drops are separate but after 5 s a significant neck region forms between the two drops with a mean height of 3.2 ± 0.5 μm, as determined by simply counting the number of fringes and using equation (1). However, to realize the goal of a full surface shape reconstruction during coalescence we must overcome problems in both the acquisition of Lloyd's fringe data and the extension of the reconstruction method to three dimensions.

The first key problem inherent in a full reconstruction of surface topography is evident from figure 5. UV radiation, incident from the bottom of the image, creates a shadowing effect and so only part of the coalescing droplets are illuminated. The shadowing problem can be simply overcome by installing multiple UV illumination sources at identical angles of incidence to the substrate, but illuminating the object at different angles. Additional sources will significantly increase the surface area illuminated by Lloyd's fringes and hence provide critically important data for the 3D reconstruction process.

It can also be observed from figures 2(a), 3(a) and 5 that the top of the droplets appears brighter than the contact-line regions due to the near grazing incidence of the illumination, which increases electron photoemission within $\bar{\ell}$ of the surface. This background intensity increases relatively slowly on the scale of a Lloyd's fringe width and so does not significantly influence the fringe position. However, in systems where the surface curvature can vary rapidly, it will be necessary to carefully subtract the background intensity by extrapolation between fringe minima either side of the peak position. This will correct for systematic fringe shifts induced by variations in background intensity.

In addition to the variation in background intensity, it can be seen in figures 3(a) and 5 that the visibility of Lloyd's fringes decreases with increasing distance from the substrate. This can be attributed to the lack of coherence of the Hg arc-discharge lamps used in our experiments and this can be improved by the use of higher coherence sources such as lasers [26]. However, despite this reduction in visibility, it is worth noting that the identification of at least

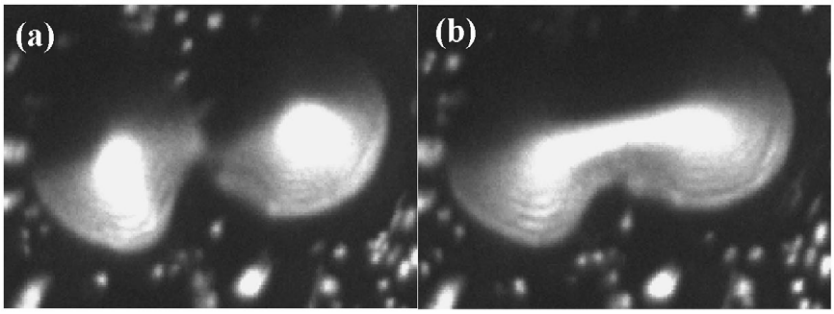

Figure 5. Images captured from a movie of Ga droplet coalescence at 640 °C. In (a) the droplets are separated. (b) After 5 s the droplets coalesce forming a neck region.

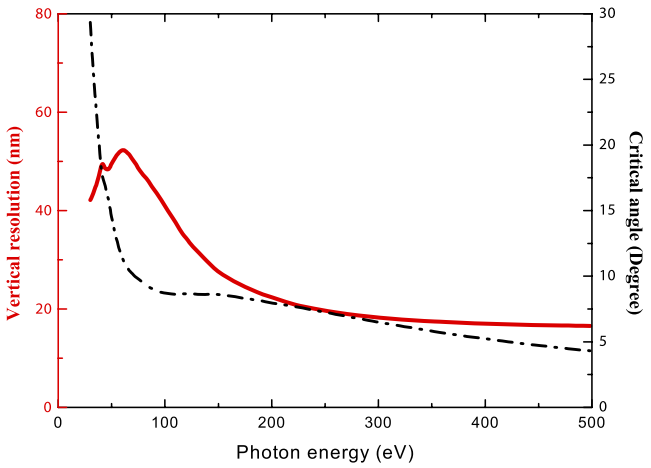

Figure 6. Critical angle of reflection and vertical resolution calculated from equation (1) as a function of photon energy.

seven fringes in figure 3(a) indicates that non-monochromatic sources, such as Hg arc-discharge lamps still represent viable sources to investigate the important droplet contact-line region (figure 3(b)). Indeed, if we successively remove the two bright fringes closest to the top of the droplet from the data, the shaded region in figure 3(b) shows the resulting variation of the reconstructed profile. The reduction in fringe number therefore does not substantially influence the reconstruction of the important contact-line region.

As discussed in section 2.1, Lloyd's fringes are distorted by the presence of a non-uniform surface electric field. A quantitative interpretation of surface shape therefore requires that we account for these distortions due to surface roughness, via equation (3). Equation (3) generalizes the Hilbert transform (4) and can in principle be used as the basis for a full 3D reconstruction of surface topography. The proximity of adjacent droplets during coalescence can give rise to complicated electric field patterns, which will inevitably complicate the reconstruction process. Furthermore, it will be important to establish how experimental measurement errors propagate through the iteration process. Nevertheless, it would seem entirely feasible to develop robust ways of inverting the generalized 'Hilbert' transform (equation (3)) to obtain the 2D island profile, $h(x, y)$ and generate 3D movies of dynamic events.

3.2. Synchrotron-based Lloyd's mirror x-ray PEEM (XPEEM)

At present the height resolution of the method is limited to ∼0.5 μm (the minimum fringe spacing) using a UV lamp source but the resolution of the technique would be considerably improved using high coherence monochromatic synchrotron UV radiation or even soft x-ray PEEM (with elemental selectivity). A plot of critical angle of total external reflection, $\theta_c = \sqrt{2\delta}$, and vertical resolution calculated from equation (1) as a function of photon energy is shown in figure 6. Here, δ is the refractive index decrement, which is related to the index of refraction $n = 1 - \delta + i\beta$, where β is the absorption index. This indicates that a resolution of $\Delta z \approx 50$ nm is obtained for an incident photon energy of 50 eV and a critical angle of 15°, corresponding to a GaAs substrate [32]. Several synchrotron-based XPEEM sites are compatible with Lloyd's mirror method and the improved resolution would open up the possibility of studying topographic shape changes on length scales approaching the nanoscale regime. In addition, the high coherence of the monochromatic source will improve the visibility of Lloyd's fringes with height [26].

Acknowledgments

We are grateful to Rod Mackie for technical support. The authors acknowledge funding from the Australian Research Council.

References

[1] Foxon C T, Harvey J A and Joyce B A 1973 *J. Phys. Chem. Solids* **89** 1693
[2] Arthur J R 1967 *J. Phys. Chem. Solids* **28** 2257
[3] Tsao J Y 1993 *Materials Fundamentals of Molecular Beam Epitaxy* (San Diego, CA: Academic)
[4] Zinke-Allmang M, Feldman L C and van Saarloos W 1992 *Phys. Rev. Lett.* **68** 2358
[5] Lowes T D and Zinke-Allmang M 1992 *J. Appl. Phys.* **73** 4937
[6] Chatillon C and Chatain D 1995 *J. Cryst. Growth* **151** 91
[7] Family F and Meakin P 1988 *Phys. Rev. Lett.* **61** 428
[8] Huang S *et al* 2006 *Appl. Phys. Lett.* **89** 031921
[9] Yamagiwa M *et al* 2006 *Appl. Phys. Lett.* **89** 113115
[10] Mano T *et al* 1999 *Japan. J. Appl. Phys.* **38** L1009
[11] Kim J S and Koguchi L 2004 *Appl. Phys. Lett.* **85** 5893
[12] Mano T and Koguchi L 2005 *J. Cryst. Growth* **278** 108
[13] Mano T *et al* 2005 *Nano Lett.* **5** 425
[14] Heyn Ch *et al* 2007 *Phys. Rev.* B **76** 075317
[15] Stranski I N and Krastanow L 1937 *Akad. Wiss. Wien, Math.-Naturwiss. Klasse* **146** 797
[16] Bauer E 1994 *Rep. Prog. Phys.* **57** 895
[17] Tromp R M and Hannon J B 2002 *Surf. Rev. Lett.* **9** 1565
[18] Altman M S, Chung W F and Liu C H 1998 *Surf. Rev. Lett.* **5** 1129
[19] Günther S, Kaulich B, Gregoratti l and Kiskinova M 2002 *Prog. Surf. Sci.* **70** 187
[20] Rotermund H H, Engel W, Jakubith S, von Oertzen A and Ertl G 1991 *Ultramicroscopy* **36** 164
[21] Swiech W, Rausenberger B, Engel W, Bradshaw A M and Zeitler E 1993 *Surf. Sci.* **294** 297
[22] Kennedy S M, Jesson D E, Morgan M J and Smith A E 2006 *Phys. Rev.* A **74** 044701
[23] Nepijko S A, Sedov N N, Schönhense G, Escher M, Bao X and Huang W 2000 *Ann. Phys.* **9** 441
[24] Rempfer G F, Nadakavukaren K K and Griffith O H 1980 *Ultramicroscopy* **5** 437
[25] Nepijko S A, Gloskovskii A, Sedov N N and Schönhense G 2003 *J. Microsc.* **211** 89
[26] Jesson D E, Pavlov K M, Morgan M J and Usher B F 2007 *Phys. Rev. Lett.* **99** 016103
[27] Born M and Wolf E 1999 *Principles of Optics* 7th edn (Cambridge: Cambridge University Press)
[28] Pawsey J L, Payne-Scott R and McCready L L 1946 *Nature* **157** 158
[29] Solak H H, He D, Li W, Singh-Gasson S, Cerrina F, Sohn B H, Yang X M and Nealy P 1999 *Appl. Phys. Lett.* **75** 2328
[30] See, for example, Gerstein E R 2002 *Am. Sci.* **90** 154
[31] Norris C N and Wotherspoon J T M 1977 *J. Phys. F: Met. Phys.* **7** 1599
[32] Henke B L *et al* 1993 X-ray interactions: photoabsorption, scattering, transmission, and reflection at $E = 50$ eV–30 000 eV, $Z = 1$–92 *At. Data Nucl. Data Tables* **54** 181–342